International Journal of the JCRM
Japanese Committee for Rock Mechanics

Volume 7, Number 1, November 2011, pp.43-48
[TECHNICAL NOTES]

Time-dependent behaviors of methane-hydrate bearing sediments in triaxial compression test

Kuniyuki MIYAZAKI*, Tsutomu YAMAGUCHI**, Yasuhide SAKAMOTO*** & Kazuo AOKI*

** Methane Hydrate Research Center, National Institute of Advanced Industrial Science and Technology, Tsukuba-shi, Ibaraki 305-8569 Japan*
*** Dept. of Environmental Science, Toho University, Funabashi-shi, Chiba 606-8501 Japan*
**** Institute for Geo-Resources and Environment, National Institute of Advanced Industrial Science and Technology, Tsukuba-shi, Ibaraki 305-8569 Japan*

Received 11 08 2011; accepted 15 10 2011

ABSTRACT

Natural gas hydrate, existing in marine sediments worldwide and in permafrost regions, is anticipated to be a promising energy resource. It is essential to consider the mechanical properties, including their time dependence, of a gas hydrate reservoir to simulate the geomechanical response to gas extraction from a reservoir. Recently it has been revealed that gas-hydrate-bearing sediments have rocklike mechanical characteristics due to the cementation effect of the hydrate between soil particles. To obtain information about the time dependence of gas-hydrate-bearing sediments, experimental methods for drained triaxial compression tests including a procedure for the preparation of artificial methane-hydrate-bearing sediment specimens have been established. Using these methods, constant-strain-rate tests and creep tests on artificial methane-hydrate-bearing sediment specimens have been conducted. In this report, the methods and results of the tests are presented, and the time-dependent behaviors of methane-hydrate-bearing sediment are discussed. On the basis of the results, the strain-rate dependence of the peak strength was examined, and it was found that the time dependence of the artificial methane-hydrate-bearing sediment is as strong as that of frozen sand and stronger than that of many other geological materials. It was also found that the creep deformation of methane-hydrate-bearing sediment is much larger than that of water-saturated sand without the hydrate. The experimental data presented in this report are expected to be used to obtain a full understanding of the deformation mechanism of methane-hydrate-bearing sediments and to formulate a constitutive equation for methane-hydrate-bearing sediments in future studies.

Keywords: Methane hydrate, Triaxial compression test, Time dependence, Strength, Strain rate, Creep, Lifetime

1. INTRODUCTION

Methane hydrate consists of cagelike crystal structures made up of hydrogen-bonded water molecules surrounding a guest molecule of methane. Because vast amounts of natural methane hydrate reservoirs exist in marine sediments worldwide and in permafrost regions, methane hydrate is anticipated to be a promising energy resource in the near future (Makogon, 1981, 1982; Kvenvolden, 1988; Kvenvolden et al., 1993).

Since the mechanical behaviors of a methane hydrate reservoir may affect the integrity of the production well, the occurrence of geohazards and the gas productivity (Collett & Dallimore, 2002; Bugge et al., 1988; Kleinberg, 2005; Sakamoto et al., 2009), the prediction of the geomechanical response to gas extraction from a reservoir is an important research issue for the sustainable production of methane hydrate. It has recently been revealed that methane-hydrate-bearing sediments have rocklike mechanical characteristics due to the cementation effect of the hydrate between soil particles. However, the time-dependent characteristics of methane-hydrate-bearing sediments have not been clarified, although they are thought to have great significance in predicting the long-term behaviors of the sediments over a time scale of decades.

It is extremely difficult to perform mechanical tests in the laboratory on natural gas-hydrate-bearing sediment samples, because gas hydrates are usually unstable under ordinary laboratory conditions and thus may dissociate during recovery, preservation, transportation and handling of the natural core. Consequently, the experimental methods for triaxial compression tests on artificial methane-hydrate-bearing sediment samples have been established and laboratory tests such as constant-strain-rate tests and creep tests have been conducted to obtain information about the time-dependent behaviors of methane-hydrate-bearing sediments.

In this report, the methods and results of the constant-strain-rate tests and creep tests are presented, and the time-dependent behaviors of methane-hydrate-bearing

sediment are discussed.

2. TESTING METHODS

2.1 Testing apparatus

The testing apparatus used for the preparation of specimens as well as for the subsequent triaxial compression tests is drawn schematically in Figure 1. The apparatus is a digital servo-controlled machine with a maximum axial load of 200 kN. The triaxial cell has a maximum pressure of 20 MPa. The temperature inside the triaxial cell can be controlled in the range of 243 K to 293 K with an accuracy of 0.5 K using an ethylene glycol aqueous solution with 50 vol% concentration as a refrigerant liquid. The refrigerant liquid is cooled by the outer cooling tank and pumped into the triaxial cell by a high-pressure pump. The refrigerant liquid also confines the specimen by a pressure of less than 20 MPa. The cell pressure, or confining pressure, is controlled by a cell pressure controller. Pore pressure can be applied by water or methane sourced from the respective cylinders. In the tests, axial load and axial displacement are measured using a 50 kN strain-gauge-type load cell and two 25 mm linear variable differential transformers (LVDTs), respectively. All experimental data is recorded by a data acquisition system every second during the tests.

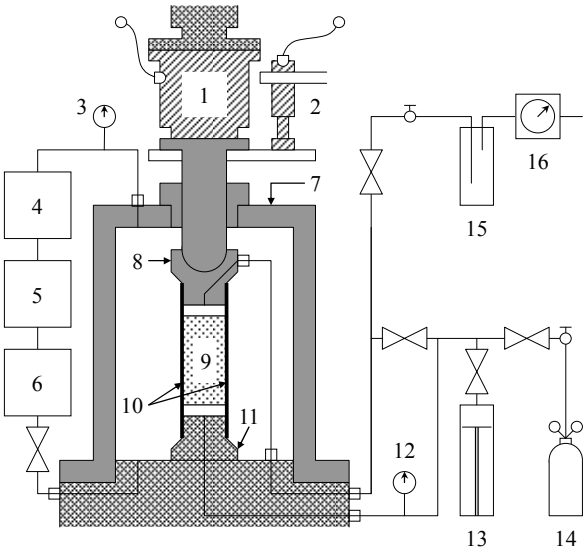

1. Load cell. 2. Displacement transducer. 3. Cell pressure gauge. 4. Cell pressure controller. 5. Refrigerant cooling tank. 6. High-pressure pump. 7. Triaxial cell. 8. Top cap. 9. Specimen. 10. Rubber membrane. 11. Pedestal. 12. Pore pressure gauge. 13. Water cylinder. 14. Methane gas cylinder. 15. Gas-water separator. 16. Gas flow meter.

Figure 1. Schematic illustration of testing apparatus.

2.2 Preparation of specimens

A host specimen was prepared by freezing a cylindrical unsaturated sand specimen by the following procedure. First, Toyoura sand (major component: SiO_2, average particle size: 230×10^{-6} m, fine fraction content: 0.0%) was compacted in a cast-iron mold filled with water on a vibration table to prepare water-saturated sand. Second, the water content was adjusted by draining excess water with a syringe pump. The water content at this moment almost completely determines the amount of methane hydrate synthesized in the specimen afterward. Third, the unsaturated sand specimen was capped with stainless-steel plates. Finally, it was placed in a 258 K freezer for over 24 h. Each host specimen was 50 mm in diameter and 100 mm in length. The porosity of the host specimens ranged from 37% to 39%, which corresponds to a relative density of 95% or more. Occasionally, finer sand such as No.7 silica sand (average particle size: 205×10^{-6} m, fine fraction content: 1.1%) or No.8 silica sand (average particle size: 130×10^{-6} m, fine fraction content: 11.5%) is used instead of Toyoura sand as the skeleton forming the host specimen. In that case, the relative density of the host specimen prepared by the above-described procedure was also found to be more than 95%.

The specimens used in the triaxial compression tests were prepared by the following procedure. First, a frozen host specimen was set in the triaxial cell. Second, a cell pressure of 1 MPa was applied and methane was made to percolate, replacing the pore air, at a temperature of 268 K or less. Third, the pore gas pressure was increased to 8 MPa at a rate of approximately 0.7 MPa/min while the cell pressure was increased to 9 MPa at the same rate. Then the temperature inside the triaxial cell was raised to 278 K. The cell pressure, pore gas pressure and temperature were then kept constant for 24 h to form methane hydrate in the pores of the host specimen. The synthesized methane hydrate is stable as a solid phase under a pore pressure of 8 MPa and a temperature of 278 K. After the formation of methane hydrate, water was injected into the specimen to replace the gaseous methane remaining in the pores of the specimen, the pedestal, the top cap, the pipework and so forth. The cell pressure, pore pressure and temperature were maintained constant during the water substitution process. Over 400×10^{-6} m^3 of water, nearly double the volume of the specimen, passed through the specimen during the substitution of water.

In this report, a water-saturated specimen of the densely packed sand sediment containing synthesized methane hydrate prepared by the above-described procedure is hereafter referred to as a "hydrate-sand specimen." "Sand specimens," i.e., water-saturated specimens of the densely packed sand sediment containing no hydrate, are also prepared by omitting the methane hydrate formation process from the above-described procedure. Figure 2 schematically shows the components of sand and hydrate-sand specimens. Note that the synthesized methane hydrate exists as a solid phase, and thus it is thought to form part of the skeleton of the specimen. Methane hydrate saturation S_h is defined as the initial volume percentage of methane hydrate in the pores of the specimen (V_{MH}/V_{void}), which can be calculated from the volume of released methane measured after the triaxial compression test. S_h is one of the most important parameters affecting the mechanical characteristics of methane-hydrate-bearing sediments. Each component of the hydrate-sand and sand specimens is distributed uniformly in a specimen according to a computed tomography image.

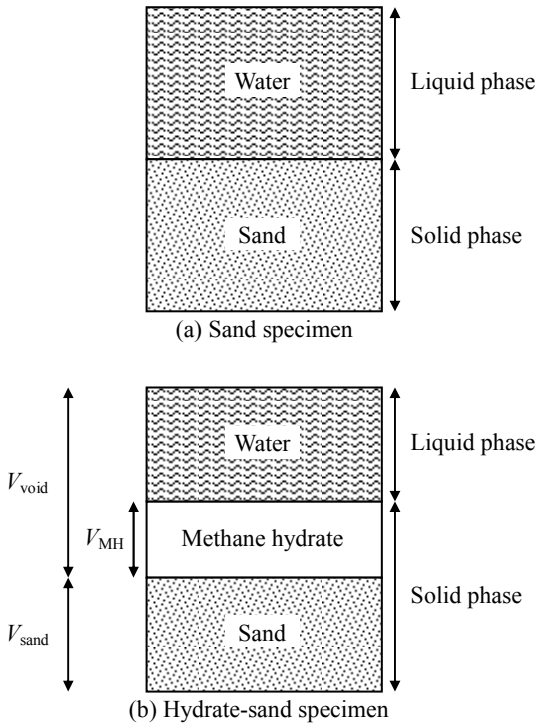

Figure 2. Schematic illustrations of component in (a) sand specimen and (b) hydrate-sand specimen.

2.3 Triaxial compression tests

Axial loading was conducted under a drained condition while maintaining the temperature at 278 K, the pore pressure at 8 MPa, the confining pressure at 9 MPa and thus the effective confining pressure σ_3', or the difference between the pore pressure and confining pressure, at 1 MPa. In this report, the results of constant-strain-rate and creep tests are presented. In the constant-strain-rate test, the strain rate C was kept constant during the axial loading process. The strain rate C and methane hydrate saturation S_h are summarized in Table 1. The average S_h for the hydrate-sand specimens used for the constant-strain-rate tests was 41%. In the creep test, the deviator stress ($\sigma_1-\sigma_3$) was increased to a predetermined creep stress σ_{cr} at a rate of 20 MPa/min, then $\sigma_1-\sigma_3$ was kept constant during axial loading. The values of σ_{cr} and S_h are summarized in Table 2. The average S_h for the hydrate-sand specimens used for the creep tests was 42%.

Table 1. Conditions of constant-strain-rate tests.

Specimen	Strain rate C, %/min	Methane hydrate saturation S_h
Sand specimen	0.1	0% (3 specimens)
	0.01	0% (3 specimens)
	0.001	0% (3 specimens)
Hydrate-sand specimen	0.1	39%, 40%, 41%, 41%
	0.05	37%, 37%, 45%
	0.01	43%, 43%
	0.005	43%
	0.001	41%, 42%

Table 2. Conditions of creep tests.

Specimen	Creep stress σ_{cr}, MPa	Methane hydrate saturation S_h
Sand specimen	3	0%*
	3.5	0%*
Hydrate-sand specimen	4	39%*, 50%*
	4.5	41%, 42%*, 42%
	5	36%, 41%, 45%, 48%
	5.5	36%, 49%, 48%

Note: the specimens that did not experience final failure are indicated by asterisks (*).

3. RESULTS

3.1 Constant-strain-rate tests

Figure 3 shows the deviator stress ($\sigma_1-\sigma_3$) plotted against the axial strain ε_a for several sand and hydrate-sand specimens. Axial strain was calculated by dividing the axial displacement measured with the LVDTs by the initial height of the specimen. In this report, a positive strain value denotes compression. $\sigma_1-\sigma_3$ increases and the slopes of the stress-strain curves, i.e., the ($\sigma_1-\sigma_3$)-ε_a curves, decrease until the deviator stress reaches a peak, and then the deviator stress decreases. In the case of the sand specimens (S_h = 0%), the stress-strain curve varies very little with the strain rate. In the case of the hydrate-sand specimens (S_h = 41%-43%), the stress-strain curve appears to vary with the strain rate; at a higher strain rate, a larger strength $(\sigma_1-\sigma_3)_{max}$ (maximum deviator stress), a larger initial slope of the stress-strain curve and more apparent strain-softening behavior are observed.

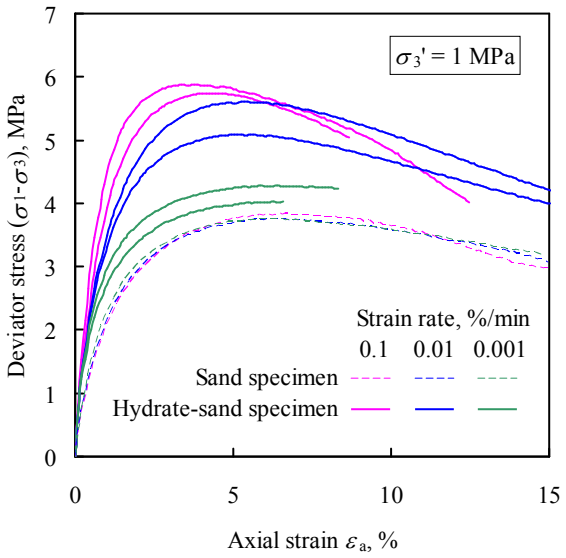

Figure 3. Deviator stress ($\sigma_1-\sigma_3$) versus axial strain ε_a in constant-strain-rate tests (Miyazaki et al., 2010).

Figure 4 shows the strength $(\sigma_1-\sigma_3)_{max}$ plotted against the strain rate C. $(\sigma_1-\sigma_3)_{max}$ for the hydrate-sand specimens increases with C, while that for the sand specimens varies

little with C. This result indicates that the time dependence of a specimen is increased when methane hydrate exists in the pores.

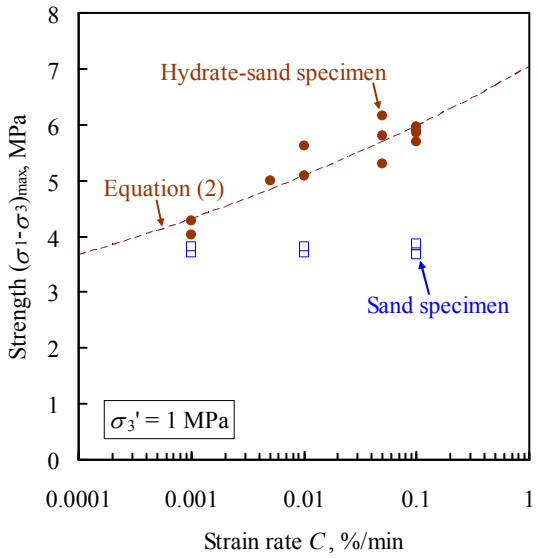

Figure 4. Strength $(\sigma_1-\sigma_3)_{max}$ versus strain rate C in constant-strain-rate tests.

The strength $(\sigma_1-\sigma_3)_{max}$ for the hydrate-sand specimens depends on S_h and C. Under the effective confining pressure σ_3' of 1 MPa, the triaxial compressive strength $(\sigma_1-\sigma_3)_{max1}$, which is obtained at a strain rate C of 0.1 %/min, can be approximated as a function of S_h by the following expression (Miyazaki et al., 2009):

$$(\sigma_1-\sigma_3)_{max1}(S_h) = (\sigma_1-\sigma_3)_{max1}(0) + \alpha S_h^{\beta}, \quad (1)$$

where $(\sigma_1-\sigma_3)_{max1}(0)$ is the strength of the sand specimen (3.5 MPa) and α and β are parameters determining how $(\sigma_1-\sigma_3)_{max1}$ increases with S_h (2.31×10^{-3} and 1.88, respectively). The strain-rate dependence of strength is often evaluated using the parameter m, where the strength is proportional to the mth power of the strain rate C. The triaxial compressive strength $(\sigma_1-\sigma_3)_{max2}$, which is obtained from the constant-strain-rate tests in this report, is approximated as a function of C by the broken curve in Figure 4 calculated using:

$$(\sigma_1-\sigma_3)_{max2}(C) = 7.03\ C^{0.071}. \quad (2)$$

The strength $(\sigma_1-\sigma_3)_{max1}$ calculated by substituting S_h = 42% into Equation (1) nearly equals to the strength $(\sigma_1-\sigma_3)_{max2}$ calculated by substituting C = 0.1%/min into Equation (2).

3.2 Creep tests

Figure 5 shows the strain rate ($d\varepsilon_{cr}/dt$) plotted against the elapsed time t for the sand and hydrate-sand specimens. A larger $d\varepsilon_{cr}/dt$ is observed at a higher σ_{cr} for both sand and hydrate-sand specimens. The slope of the log($d\varepsilon_{cr}/dt$)-log(t) relationship for each sand specimen is approximately −1, indicating that the creep behavior of a sand specimen almost follows a logarithmic law, while that for hydrate-sand specimens in the primary creep region ranges from −0.7 to −0.4. The creep stress level σ_{cr}*, or the creep stress normalized by $(\sigma_1-\sigma_3)_{max1}$ given by Equation (1), can be expressed as

$$\sigma_{cr}^* = \sigma_{cr} / (\sigma_1-\sigma_3)_{max1}. \quad (3)$$

According to Equations (1) and (3), for example, $(\sigma_1-\sigma_3)_{max1}$ for the sand specimen (S_h = 0%) and the hydrate-sand specimen with S_h of 42% are 3.54 MPa and 6.12 MPa, respectively. Thus a σ_{cr} of 3.5 MPa for a sand specimen corresponds to a σ_{cr}* of 99% and a σ_{cr} of 4.5 MPa for a hydrate-sand specimen with an S_h of 42% corresponds to a σ_{cr}* of 74%. Equation (1) was derived from the triaxial compressive strength at a strain rate of 0.1%/min, whereas the deviator stress was increased at a stress rate of 20 MPa/min in the creep test; the loading rate in creep tests was considerably faster than that in constant-strain-rate tests. Thus, it is possible that a σ_{cr} is more than 100%.

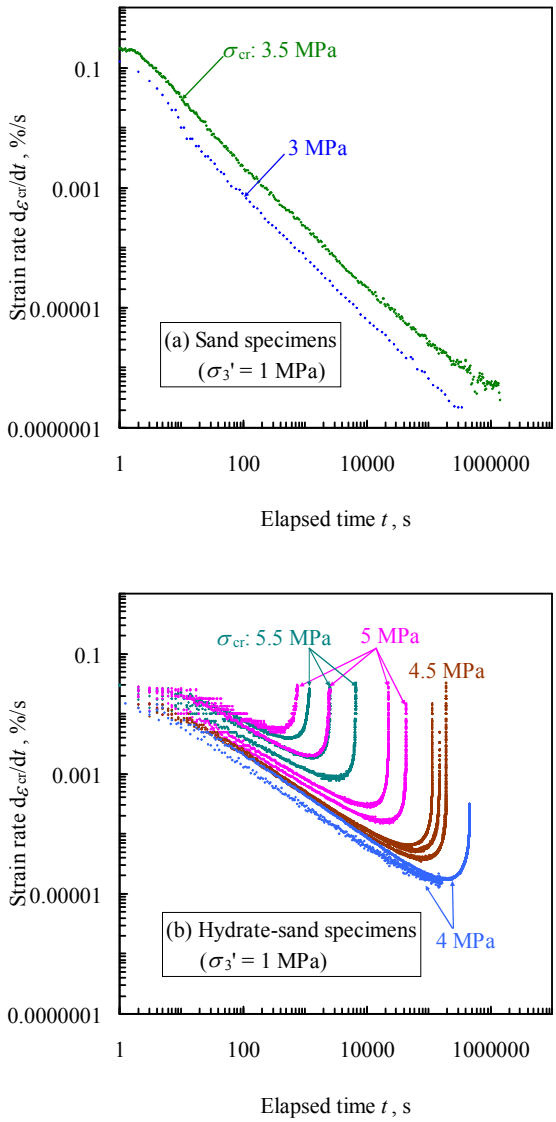

Figure 5 Strain rate ($d\varepsilon_{cr}/dt$) versus elapsed time t for (a) sand specimens and (b) hydrate-sand specimens.

As can be seen in Figure 5, the sand specimen under a σ_{cr} of 3.5 MPa, or under a σ_{cr}* of 94%, does not experience tertiary creep, whereas the three hydrate-sand specimens with S_h of 41%-42% under a σ_{cr} of 4.5 MPa, or under a σ_{cr}* of

78%-80%, exhibit tertiary creep, suggesting that the time-dependent behavior of a hydrate-sand specimen is more apparent than that of a sand specimen, as is indicated by the results of the constant-strain-rate tests.

Figure 6 shows the creep lifetime t_{crf} plotted against the creep stress level σ_{cr}* for the hydrate-sand specimens that experienced final failure. Although a large variation can be seen, t_{crf} tends to decrease with increasing σ_{cr}*.

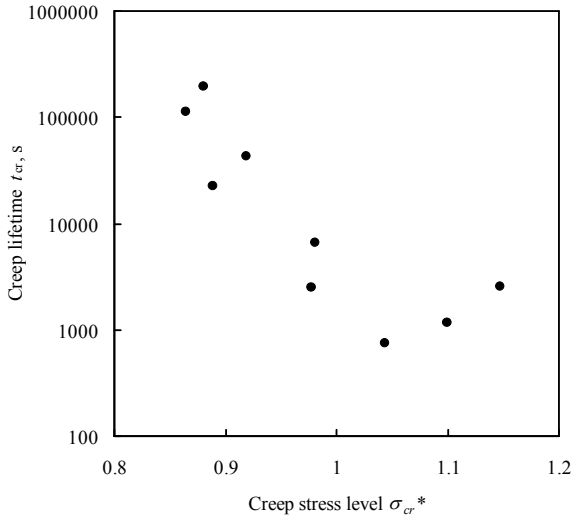

Figure 6 Creep lifetime t_{cr} versus creep stress level σ_{cr}* for hydrate-sand specimens.

4. COMPARISON OF TIME DEPENDENCE WITH OTHER MATERIALS

From Equation (2), the strength of a hydrate-sand specimen was found to be proportional to the strain rate raised to a power of approximately 0.071, suggesting that the hydrate-sand specimen has considerably stronger time dependence than rocks, sands and other geomaterials. One of the most important findings of our research is that the time dependence of a specimen greatly depends on whether or not it contains methane hydrate. Although the deformation mechanism is not yet fully understood, it can be concluded that the methane hydrate forming the skeleton of the hydrate-sand specimen is closely related to the deformation mechanism underlying its time-dependent behaviors. This finding indicates that care must be taken when predicting the mechanical behaviors of a methane hydrate reservoir during the exploitation of reservoirs. Thus, in future, a constitutive equation that takes into account the strong time dependence of hydrate-sand specimens should be formulated.

Table 3 shows the test conditions and results of some previous studies on the loading-rate dependence of the strength of several materials such as ice, methane hydrate and frozen sand (Miyazaki et al., 2010). The value of m for ice was 0.15 to 0.25 in earlier works (Hawkes & Mellor, 1972; Jones, 1982; Cole, 1987; Jones, 1997), indicating a reasonably strong strain-rate dependence, although these works were performed under different experimental parameters, such as the material, temperature, stress state, testing method, range of strain rate and so forth. There have been very few studies on the strain-rate dependence of methane hydrate. Hyodo et al. (2002, 2005) investigated the strain-rate dependence of the triaxial compressive strength of an artificial specimen of compacted granular methane hydrate and reported that the strain-rate dependence was slightly stronger than that of ice. Compared with the results reported in earlier works, the strain-rate dependence of the strength, or the time-dependence, of the hydrate-sand specimen obtained in this study appears to be slightly lower than that of ice or compacted granular methane hydrate.

As can be seen in Table 3, the value of m for frozen sand was 0.07 to 0.1 (Parameswaran, 1980; Sayles & Epanchin, 1966; Sayles, 1974; Parameswaran & Jones, 1981) in most cases, indicating a nearly equal strain-rate dependence to that of the hydrate-sand specimen. There have been very few studies on the strain-rate dependence of sediments containing hydrates. Parameswaran et al. (1989) studied a frozen sand specimen containing tetrahydrofuran hydrate (THF hydrate) and reported that m was equal to 0.010 according to the results of uniaxial compression tests, indicating a weaker strain-rate dependence than those of frozen sand without hydrates and the hydrate-sand specimens in this study.

For frozen sand, a convincing mechanism explaining its reasonably strong strain-rate dependence was proposed in an

Table 3. Earlier works on strain-rate dependence of strength.

Author(s)	Material	Loading condition	Temperature, °C	Strain rate, s^{-1}	m
Hawkes & Mellor (1972)	Polycrystalline ice	Uniaxial compression	-7	10^{-5} to 10^{-2}	0.16
		Uniaxial tension	-7	10^{-5} to 10^{0}	–
Jones (1982)	Polycrystalline ice	Triaxial compression	-11	10^{-7} to 10^{-1}	0.25
		Uniaxial compression	-11	10^{-7} to 10^{-1}	0.2
Cole (1987)	Polycrystalline ice	Uniaxial compression	-5	10^{-7} to 10^{-1}	0.23
Jones (1997)	Freshwater ice	Uniaxial compression	-11	10^{-1} to 10^{1}	0.15
	Baltic sea ice	Uniaxial compression	-11	10^{-1} to 10^{1}	0.19
Hyodo et al. (2005)	Compressed granular methane hydrate	Triaxial compression	-30	1.67×10^{-6} to 1.67×10^{-5}	–
Parameswaran (1980)	Frozen saturated Ottawa sand	Uniaxial compression	-6	10^{-7} to 10^{-2}	0.073
			-10	10^{-7} to 10^{-2}	0.071
			-15	10^{-7} to 10^{-2}	0.079
Sayles & Epanchin (1966)	Frozen saturated Ottawa sand	Uniaxial compression	-3	1.67×10^{-4} to 2×10^{-2}	0.105
			-6.5	1.67×10^{-4} to 2×10^{-2}	0.092
			-10	1.67×10^{-4} to 2×10^{-2}	0.094
Sayles (1974)	Frozen saturated Ottawa sand	Triaxial compression	-3.85	1.67×10^{-5} to 1.67×10^{-2}	0.1
Parameswaran & Jones (1981)	Frozen saturated Ottawa sand	Triaxial compression	-12	10^{-5} to 10^{-2}	0.08
Parameswaran et al. (1989)	Frozen sand containing THF hydrate	Uniaxial compression	-6	10^{-6} to 10^{-3}	0.01

earlier work; it was presumed by Parameswaran (1980) that the strain-rate dependence is governed by the liquid phase around the sand grains, namely, a quasi-liquid layer, and that this phase is associated with the melting of ice under pressure at the points where it is in contact with grains. Methane hydrate resembles ice in the sense that it is mainly formed by hydrogen bonding. Thus, in the hydrate-sand specimens, a similar phenomenon may occur, resulting in the reasonably strong time-dependence. Further research is needed to clarify the mechanism explaining the strong time-dependence for the hydrate-sand specimens.

5. SUMMARY

In this report, the methods and results of constant-strain-rate tests and creep tests on artificial methane-hydrate-bearing sediment specimens under triaxial compression were presented and the time-dependent behaviors were discussed. According to the test results, the sand specimens had very weak time dependence, suggesting that the time dependence is negligible in most cases; on the other hand, the hydrate-sand specimens had considerable time dependence, suggesting that the methane hydrate in the pores among the sand particles affects the time-dependent behavior of methane-hydrate-bearing sediments. The strain-rate dependence of the hydrate-sand specimens was as strong as that of frozen sand and stronger than that of the sand specimens in this study and many other geomaterials. However, it was weaker than that of ice and methane hydrate. These findings are expected to be used to obtain a full understanding of the deformation mechanism of methane-hydrate-bearing sediments and to formulate a constitutive equation for methane-hydrate-bearing sediments in future studies.

ACKNOWLEDGMENTS

This work was financially supported by the Research Consortium for Methane Hydrate Resources in Japan (MH21 Research Consortium) in the Japan's Methane Hydrate R&D Program by the Ministry of Economy, Trade and Industry (METI). The authors would like to thank Mr. Takao Ohno for help in conducting the experiments.

REFERENCES

Bugge, T., Belderson, R.H., & Kenyon, N.H., 1988. The Storegga Slide, *Philosophical Transactions of the Royal Society of London A*, **325**, pp.357-388.

Cole, D.M., 1987. Strain-rate and Grain-size Effects in Ice, *Journal of Glaciology*, **33**, No.155, pp.274-280.

Collett, T.S. & Dallimore, S.R., 2002. Detailed Analysis of Gas Hydrate Induced Drilling and Production Hazards, *Proceedings of 4th International Conference on Gas Hydrates*, **1**, pp.47-52.

Hawkes, I. & Mellor, M., 1972. Deformation and Fracture of Ice under Uniaxial Stress, *Journal of Glaciology*, **11**, No.61, pp.103-131.

Hyodo, M., Hyde, A.F.L., Nakata, Y., Yoshimoto, N., Fukunaga, M., Kubo, K., Nanjo, Y., Matsuo, T., & Nakamura, K., 2002. Triaxial Compressive Strength of Methane Hydrate, *Proceedings of 12th International Offshore and Polar Engineering Conference*, pp.422-428.

Hyodo, M., Nakata, Y., Yoshimoto, N., & Ebinuma, T., 2005. Basic Research on the Mechanical Behavior of Methane Hydrate-sediments Mixture, *Soil and Foundation*, **45**, pp.75-85.

Jones, S.J., 1982. The Confined Compressive Strength of Polycrystalline Ice, *Journal of Glaciology*, **28**, No.98, pp.171-177.

Jones, S.J., 1997. High Strain-rate Compression Tests on Ice, *The Journal of Physical Chemistry B*, **101**, No.32, pp.6099-6101.

Kleinberg, R.L., 2005. Mechanical Stability of Seafloor Sediments with Application to Gas Hydrate Dposits, *Proceedings of 5th International Conference on Gas Hydrates*, **3**, pp.736-748.

Kvenvolden, K.A., 1988. A Major Reservoir of Carbon in the Shallow Geosphere?, *Chemical Geology*, **71**, No.1-3, pp.41-51.

Kvenvolden, K.A., Ginsburg, G.D., & Soloviev, V.A., 1993. Worldwide Distribution of Subaquatic Gas Hydrates, *Geo-Marine Letters*, **13**, No.1, pp.32-40.

Makogon, Y.F., 1981. *Hydrates of Natural Gas*, Tulsa, Pennwell Publishing Company.

Makogon, Y.F., 1982. Perspectives for the Development of Gas-hydrate Deposits, *Proceedings of 4th Canadian Permafrost Conference*, pp.299-304.

Miyazaki, K., Yamaguchi, T., Sakamoto, Y., Haneda, H., Ogata, Y., Aoki, K., & Okubo, S., 2009. Creep of Sediment Containing Synthetic Methane Hydrate, *Journal of MMIJ*, **125**, pp.156-164. (in Japanese)

Miyazaki, K., Masui, A., Aoki, K., Sakamoto, Y., Yamaguchi., T, & Okubo, S., 2010. Strain-Rate Dependence of Triaxial Compressive Strength of Artificial Methane-Hydrate-Bearing Sediment, *International Journal of Offshore and Polar Engineering*, **20**, No.4, pp.256-264.

Parameswaran, V.R., 1980. Deformation Behaviour and Strength of Frozen Sand, *Canadian Geotechnical Journal*, **17**, No.1, pp.74-88.

Parameswaran, V.R. & Jones, S.J., 1981. Triaxial Testing of Frozen Sand, *Journal of Glaciology*, **27**, No.95, pp.147-155.

Parameswaran, V.R., Paradis, M., & Handa, Y.P., 1989. Strength of Frozen Sand Containing Tetrahydrofuran Hydrate, *Canadian Geotechnical Journal*, **26**, No.3, pp.479-483.

Sakamoto, Y., Kakumoto, M., Miyazaki, K., Tenma, N., Komai, T., & Yamaguchi, T., 2009. Numerical Study on Dissociation of Methane Hydrate and Gas Production Behavior in Laboratory-scale Experiments for Depressurization: Part 3 -Numerical Study on Estimation of Permeability in Methane Hydrate Reservoir-, *International Journal of Offshore and Polar Engineering*, **19**, pp.124-134.

Sayles, F.H. & Epanchin, N.V., 1966. Rate of Strain Compression Tests on Frozen Ottawa Sand and Ice, *US Army CRREL Technical Note*.

Sayles, F.H., 1974. Triaxial Constant Strain Rate Tests and Triaxial Creep Tests on Frozen Ottawa Sand, *US Army CRREL Technical Report*, No.253.